Berezinskii-Kosterlitz-Thouless transition in lattice Schwinger model with one flavor of Wilson fermion

Yuya Shimizu[1] and Yoshinobu Kuramashi[2,1]

[1]*RIKEN Advanced Institute for Computational Science, Kobe, Hyogo 650-0047, Japan*
[2]*Center for Computational Sciences, University of Tsukuba, Tsukuba, Ibaraki 305-8577, Japan*

We have made a detailed study of the phase structure for the lattice Schwinger model with one flavor of Wilson fermion on the (m, g) plane. For numerical investigation, we develop a decorated tensor renormalization method for lattice gauge theories with fermions incorporating the Grassmann tensor renormalization. Our algorithm manifestly preserves rotation and reflection symmetries. We find not only a parity-broken phase but also a Berezinskii-Kosterlitz-Thouless (BKT) transition by evaluating the central charge and an expectation value of a projection operator into the parity-odd subspace. The BKT phase boundaries converge into the degenerated doubler pole $(m, g) = (-2, 0)$, while the parity-breaking transition line ends at the physical pole $(m, g) = (0, 0)$. In addition, our analysis of scaling dimensions indicates that a conformal field theory with SU(2) symmetry arises on the line of $m = -2$.

I. INTRODUCTION

The Wilson fermion is one of the standard lattice regularizations for the continuum Dirac fermion, avoiding the species-doubling problem. Although the chiral symmetry is explicitly broken in this formulation, the existence of massless pseudoscalar mesons is expected by Aoki's scenario for even numbers of flavors as gapless modes accompanied by a parity-flavor-breaking transition (see a summary report [1]). On the other hand, the phase structure of the Wilson fermion with odd numbers of flavors is not fully understood yet. The condition of the Vafa-Witten theorem [2] is not fulfilled in this case and the parity symmetry itself can be spontaneously broken, that is, the flavor singlet pseudoscalar meson can be also massless. In fact, analyses based on the strong-coupling expansion show that the parity symmetry is really broken. A possible answer was indicated by numerical simulations for three flavor lattice QCD: The redundant phase is restricted within the strong-coupling region and the correct continuum physics can be realized in a weak-coupling region [3]. However, it is still quite hard to investigate the parity- or parity-flavor-breaking transition, because Monte Carlo approaches suffer from the numerical sign problem in the broken phase for odd numbers of flavors.

As a first step toward a long-term goal to understand the phase structure of odd numbers of flavors of the Wilson fermion completely, we study the lattice Schwinger model with one flavor of the Wilson fermion. The Schwinger model, two-dimensional QED, is simple but shares several properties with QCD. It was numerically verified by several methods at a high level of precision that an Ising transition occurs in the strong-coupling limit [4–6]. Moreover, we showed that such a transition is retained even at finite couplings and the transition line approaches the physical pole $(m, g) = (0, 0)$ where m is the fermion mass and g is the gauge coupling [6]. On the other hand, the situation of the lattice Schwinger model around $m = -2$ is not clear yet. In the strong coupling limit of $g = \infty$, as discussed by Salmhofer, it is mapped to a critical six-vertex model whose criticality is described by a conformal field theory (CFT) with the central charge $c = 1$ [7]. In the free limit, the point of $(m, g) = (-2, 0)$ corresponds to the degenerated doubler pole, which is governed by the CFT with $c = \frac{1}{2} + \frac{1}{2} = 1$. A natural expectation may be an existence of a $c = 1$ CFT line or region between $(m, g) = (-2, 0)$ and $(m, g) = (-2, \infty)$, which should be confirmed by a detailed investigation of the phase structure around $m = -2$ at finite couplings by using a reliable numerical method.

In order to investigate the phase structure of the lattice Schwinger model with one flavor of the Wilson fermion throughout the (m, g) plane, we have improved our method proposed in Ref. [6], which was based on the tensor renormalization group (TRG) [8]. The TRG is one of the so-called tensor network algorithms, which are free from the sign problem, and is suitable for computation of classical partition functions and quantum path integrals. It was

originally developed mainly in the fields of condensed matter physics and quantum information science. In recent years, however, it has also attracted a lot of attention in high energy physics and there have already been many applications to lattice field theories [6,9–21]. Although our previous method succeeded in clear demonstration of the Ising transition at finite couplings by adopting a Grassmann version of the TRG proposed by Gu and others [22], the gauge redundancy demanded increasing bond dimensions of tensor to keep numerical precisions at finite couplings. After our work in Refs. [6,13], Dittrich and others proposed a variation of the TRG method that gives a better control of the gauge redundancy by introducing an additional structure decorating the tensor network [14]. In this paper we develop a more efficient method to study the lattice Schwinger model with one flavor of the Wilson fermion by combining the ideas of the decorated TRG and Grassmann TRG, and investigate the phase structure in the region around $m = -2$ at finite couplings, which was out of reach in previous studies.

It is worth noting that other tensor network methods are also gathering much attention from the field of high energy physics. They also choose the analysis of the lattice Schwinger model as a pilot study, though the Kogut-Susskind fermion formulation has been employed so far in all such works [23–36].

The layout of this papers is as follows. In Sec. II, we explain the application of our decorated tensor renormalization to the lattice Schwinger model with one flavor of the Wilson fermion. Section III presents the results for numerical investigation of the phase structure. Finally we summarize our paper in Sec. IV.

II. DECORATED TENSOR RENORMALIZATION FOR THE LATTICE SCHWINGER MODEL

A. Lattice Schwinger model with one flavor of the Wilson fermion

We follow the lattice formulation of the Schwinger model given in Ref. [6], but use m and g as parameters in the model throughout this paper instead of the hopping parameter κ and the inverse coupling squared β. We give the formulation again in the following to make the paper self-contained.

The Wilson-Dirac matrix is given by

$$
\begin{aligned}
\bar{\psi} D[U] \psi = (m+2) \sum_{n,\alpha} \bar{\psi}_{n,\alpha} \psi_{n,\alpha} \\
- \frac{1}{2} \sum_{n,\mu,\alpha,\beta} \bar{\psi}_{n,\alpha} [(1-\gamma_\mu)_{\alpha,\beta} U_{n,\mu} \psi_{n+\hat{\mu},\beta} \\
+ (1+\gamma_\mu)_{\alpha,\beta} U_{n-\hat{\mu},\mu}^\dagger \psi_{n-\hat{\mu},\beta}],
\end{aligned}
\tag{1}
$$

where ψ_n and $\bar{\psi}_n$ are two-component Grassmann variables at site n and $U_{n,\mu}$ is a $U(1)$ link variable at site n along the μ direction. α and β denote the Dirac indices and $\hat{\mu}$ represents a unit vector along the μ direction. The gamma matrices are

$$
\gamma_1 = \begin{pmatrix} 1 & 0 \\ 0 & -1 \end{pmatrix}, \qquad \gamma_2 = \begin{pmatrix} 0 & 1 \\ 1 & 0 \end{pmatrix}.
\tag{2}
$$

Following Ref. [7], we employ another basis,

$$
\chi_{n,1} = \frac{1}{\sqrt{2}}(\psi_{n,1}+\psi_{n,2}), \quad \chi_{n,2} = \frac{1}{\sqrt{2}}(\psi_{n,1}-\psi_{n,2}), \tag{3}
$$

$$
\bar{\chi}_{n,1} = \frac{1}{\sqrt{2}}(\bar{\psi}_{n,1}+\bar{\psi}_{n,2}), \quad \bar{\chi}_{n,2} = \frac{1}{\sqrt{2}}(\bar{\psi}_{n,1}-\bar{\psi}_{n,2}), \tag{4}
$$

only in the second (space) direction, while keeping $\{\psi_{n,\alpha}\}$ and $\{\bar{\psi}_{n,\alpha}\}$ in the first (time) direction. Using this trick, the hopping terms are simply rewritten as

$$
\sum_{\alpha,\beta} \bar{\psi}_{n,\alpha}(1+\gamma_1)_{\alpha,\beta}\psi_{n-\hat{1},\beta} = 2\bar{\psi}_{n,1}\psi_{n-\hat{1},1}, \tag{5}
$$

$$
\sum_{\alpha,\beta} \bar{\psi}_{n,\alpha}(1-\gamma_1)_{\alpha,\beta}\psi_{n+\hat{1},\beta} = 2\bar{\psi}_{n,2}\psi_{n+\hat{1},2}, \tag{6}
$$

$$
\sum_{\alpha,\beta} \bar{\psi}_{n,\alpha}(1+\gamma_2)_{\alpha,\beta}\psi_{n-\hat{2},\beta} = 2\bar{\chi}_{n,1}\chi_{n-\hat{2},1}, \tag{7}
$$

$$
\sum_{\alpha,\beta} \bar{\psi}_{n,\alpha}(1-\gamma_2)_{\alpha,\beta}\psi_{n+\hat{2},\beta} = 2\bar{\chi}_{n,2}\chi_{n+\hat{2},2}. \tag{8}
$$

Each Grassmann variable satisfies the anticommutation relations,

$$
[\psi_{n,\alpha},\bar{\psi}_{m,\beta}]_+ \equiv \psi_{n,\alpha}\bar{\psi}_{m,\beta} + \bar{\psi}_{m,\beta}\psi_{n,\alpha} = 0, \tag{9}
$$

$$
[\psi_{n,\alpha},\psi_{m,\beta}]_+ = [\bar{\psi}_{n,\alpha},\bar{\psi}_{m,\beta}]_+ = 0, \tag{10}
$$

$$
[\chi_{n,\alpha},\bar{\chi}_{m,\beta}]_+ = [\chi_{n,\alpha},\chi_{m,\beta}]_+ = [\bar{\chi}_{n,\alpha},\bar{\chi}_{m,\beta}]_+ = 0, \tag{11}
$$

and the integration rules,

$$
\int d\psi_{n,\alpha}1 = \int d\bar{\psi}_{n,\alpha}1 = 0, \tag{12}
$$

$$
\int d\psi_{n,\alpha}\psi_{m,\beta} = \int d\bar{\psi}_{n,\alpha}\bar{\psi}_{m,\beta} = \delta_{n,m}\delta_{\alpha,\beta}, \tag{13}
$$

$$
\int d\chi_{n,\alpha}1 = \int d\bar{\chi}_{n,\alpha}1 = 0, \tag{14}
$$

$$
\int d\chi_{n,\alpha}\chi_{m,\beta} = \int d\bar{\chi}_{n,\alpha}\bar{\chi}_{m,\beta} = \delta_{n,m}\delta_{\alpha,\beta}. \tag{15}
$$

Turning to the gauge part, the $U(1)$ plaquette action is given by

$$
S_g[U] = -\frac{1}{g^2} \sum_{\text{all plaquette}} \cos\varphi_p, \tag{16}
$$

$$
\varphi_p \equiv \varphi_{n,1} + \varphi_{n+\hat{1},2} - \varphi_{n+\hat{2},1} - \varphi_{n,2}, \tag{17}
$$

$$
\varphi_{n,1}, \varphi_{n+\hat{1},2}, \varphi_{n+\hat{2},1}, \varphi_{n,2} \in [-\pi,\pi], \tag{18}
$$

where $\varphi_{n,1}, \varphi_{n+\hat{1},2}, \varphi_{n+\hat{2},1}$ and $\varphi_{n,2}$ are phases of link variables that compose a plaquette variable φ_{p}.

B. Decorated tensor network representation

We transform the partition function,

$$Z = \int \mathcal{D}U \det D[U] e^{-S_{\mathrm{g}}[U]}, \tag{19}$$

into a decorated tensor network form. First, by using Eqs. (9)–(11), the fermionic part is expanded as follows:

$$\det D[U] = \prod_{n,\alpha} \left(\int \mathrm{d}\psi_{n,\alpha} \mathrm{d}\bar{\psi}_{n,\alpha} \right) e^{\bar{\psi}D[U]\psi} \tag{20}$$

$$= P_0 \int \prod_n W_n \prod_\mu H_{n,\mu}, \tag{21}$$

$$W_n \equiv (m+2)^2 + (m+2)\mathrm{d}\psi_{n,1}\mathrm{d}\bar{\psi}_{n,1}$$
$$+ (m+2)\mathrm{d}\psi_{n,2}\mathrm{d}\bar{\psi}_{n,2} + \mathrm{d}\psi_{n,1}\mathrm{d}\bar{\psi}_{n,1}\mathrm{d}\psi_{n,2}\mathrm{d}\bar{\psi}_{n,2}, \tag{22}$$

$$H_{n,1} \equiv 1 + U_{n,1}^\dagger \psi_{n,1}\bar{\psi}_{n+\hat{1},1} + U_{n,1}\psi_{n+\hat{1},2}\bar{\psi}_{n,2}$$
$$+ \psi_{n+\hat{1},2}\bar{\psi}_{n+\hat{1},1}\bar{\psi}_{n,2}\psi_{n,1}, \tag{23}$$

$$H_{n,2} \equiv 1 + U_{n,2}^\dagger \chi_{n,1}\bar{\chi}_{n+\hat{2},1} + U_{n,2}\psi_{n+\hat{2},2}\bar{\chi}_{n,2}$$
$$+ \bar{\chi}_{n+\hat{2},1}\chi_{n+\hat{2},2}\chi_{n,1}\bar{\chi}_{n,2}, \tag{24}$$

where P_0 represents a projection to terms without any Grassmann variable. Next, we perform the character expansion for the gauge part,

$$e^{\frac{1}{g^2}\cos\varphi_{\mathrm{p}}} = \sum_{b_{\mathrm{p}}=-\infty}^\infty e^{ib_{\mathrm{p}}\varphi_{\mathrm{p}}} I_{b_{\mathrm{p}}}\left(\frac{1}{g^2}\right) \tag{25}$$

$$\simeq \sum_{b_{\mathrm{p}}=-N_{\mathrm{ce}}}^{N_{\mathrm{ce}}} e^{ib_{\mathrm{p}}\varphi_{\mathrm{p}}} I_{b_{\mathrm{p}}}\left(\frac{1}{g^2}\right), \tag{26}$$

with $I_{b_{\mathrm{p}}}$ being the modified Bessel function. The truncation number N_{ce} is introduced in order to obtain a finite-dimensional tensor network [10]. Integrating out all link variables, we obtain

$$\int_{-\pi}^\pi \frac{d\varphi_{n,1}}{2\pi} H_{n,1} e^{i(b_i-b_j)\varphi_{n,1}}$$
$$= \begin{cases} 1 + \psi_{n+\hat{1},2}\bar{\psi}_{n+\hat{1},1}\bar{\psi}_{n,2}\psi_{n,1}, & b_i = b_j \\ \psi_{n,1}\bar{\psi}_{n+\hat{1},1}, & b_i = b_j + 1 \\ \psi_{n+\hat{1},2}\bar{\psi}_{n,2}, & b_i = b_j - 1 \\ 0, & \text{others} \end{cases}. \tag{27}$$

Integration for $H_{n,2}$ is performed likewise. Multiplying W_n by these integrated results yields a decorated tensor network form of the partition function,

$$Z = \int \sum_{b_1,b_2,b_3,\cdots} \sum_{i,j,k,\cdots} \mathcal{T}_{n;i,j,k,l}^{(b_1,b_2,b_3,b_4)} \mathcal{T}_{n+\hat{1};m,o,i',p}^{(b_5,b_4,b_1,b_6)}$$
$$\times \mathcal{T}_{n+\hat{2};q,r,s,j'}^{(b_7,b_3,b_8,b_1)} \cdots \mathcal{G}_{n,1;i',i}^{(b_1,b_4)} \mathcal{G}_{n,2;j',j}^{(b_3,b_1)} \cdots, \tag{28}$$

$$\mathcal{T}_{n;i,j,k,l}^{(b_1,b_2,b_3,b_4)} \equiv T_{i,j,k,l}^{(b_1,b_2,b_3,b_4)} \mathrm{d}\psi_{n,1}^{R(b_1-b_4)+p(i)} \mathrm{d}\bar{\psi}_{n,2}^{R(b_4-b_1)+p(i)}$$
$$\times \mathrm{d}\bar{\chi}_{n,2}^{R(b_1-b_3)+p(j)} \mathrm{d}\chi_{n,1}^{R(b_3-b_1)+p(j)} \mathrm{d}\bar{\psi}_{n,1}^{R(b_3-b_2)+p(k)}$$
$$\times \mathrm{d}\psi_{n,2}^{R(b_2-b_3)+p(k)} \mathrm{d}\chi_{n,2}^{R(b_4-b_2)+p(l)} \mathrm{d}\bar{\chi}_{n,1}^{R(b_2-b_4)+p(l)}, \tag{29}$$

$$\mathcal{G}_{n,1;i',i}^{(b_1,b_4)} \equiv h_{i',i}^{(b_1,b_4)} \psi_{n,1}^{R(b_1-b_4)+p(i)} \bar{\psi}_{n+\hat{1},1}^{R(b_1-b_4)+p(i')}$$
$$\times \psi_{n+\hat{1},2}^{R(b_4-b_1)+p(i')} \bar{\psi}_{n,2}^{R(b_4-b_1)+p(i)}, \tag{30}$$

$$\mathcal{G}_{n,2;j',j}^{(b_3,b_1)} \equiv h_{j',j}^{(b_3,b_1)} \chi_{n,1}^{R(b_3-b_1)+p(j)} \bar{\chi}_{n+\hat{2},1}^{R(b_3-b_1)+p(j')}$$
$$\times \chi_{n+\hat{2},2}^{R(b_1-b_3)+p(j')} \bar{\chi}_{n,2}^{R(b_1-b_3)+p(j)}. \tag{31}$$

$T^{(b_1,b_2,b_3,b_4)}$ is a decorated tensor kernel that includes no Grassmann number and its detail is given in Appendix A. $h_{i',i}^{(b_1,b_4)}$ is equal to the Kronecker delta $g_{i',i}$ for the initial tensor network. R is a ramp function that satisfies

$$R(x) = \begin{cases} x, & x \geq 0 \\ 0, & x < 0 \end{cases}. \tag{32}$$

$p(i)$ equals 0 (1) when i indicates a parity-even (-odd) state under a reflection. Note that $\{\psi_{n,\alpha}\}$, $\{\chi_{n,\alpha}\}$ and others are treated as independent variables. Figure 1 illustrates Eq. (28) as a network diagram.
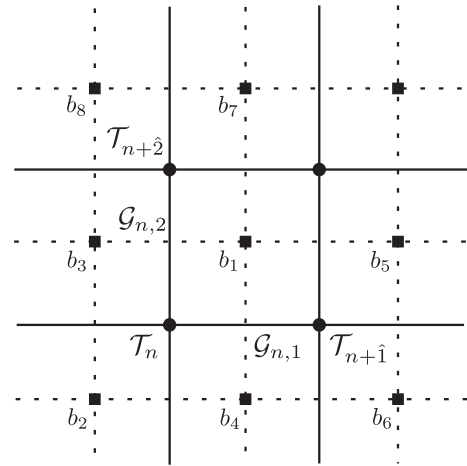

FIG. 1. Schematic representation of the decorated tensor network of Eq. (28). Each site indicated by a filled circle represents each decorated tensor $\mathcal{T}_n$. $\{\mathcal{G}_{n,\mu}\}$ are assigned to each link. The decoration labels $\{b_i\}$ sit on each plaquette.

C. Decorated TRG procedure

One TRG cycle consists of two steps, decomposing each tensor in Eq. (28) by using the singular value decomposition (SVD) and contracting the decomposed tensors to obtain coarse-grained tensors. We extend an algorithm proposed in Ref. [14] to systems including fermions. Fermionic degrees of freedom are treated by following our previous approach given in Ref. [6], but some modifications are introduced to preserve rotation and reflection symmetries.

First, let us explain the decomposition part. A matrix form of the decorated tensor kernel $T^{(b_1,b_2,b_3,b_4)}$ is defined as follows:

$$M^{(b_3,b_4)}_{(b_1;i,j),(b_2;k,l)} \equiv T^{(b_1,b_2,b_3,b_4)}_{i,j,k,l}. \tag{33}$$

Then, we perform the SVD,

$$M^{(b_3,b_4)}_{(b_1;i,j),(b_2;k,l)} = \sum_m U^{(b_3,b_4)}_{(b_1;i,j),m} \sigma^{(b_3,b_4)}_m V^{(b_3,b_4)}_{m,(b_2;k,l)}. \tag{34}$$

Only the largest D singular values out of $\{\sigma^{(b_3,b_4)}_m\}$ are kept and others are approximated to 0. When $b_3 = b_4$, $M^{(b_3,b_4)}$ is a symmetric matrix and the eigenvalue decomposition is

applied rather than the SVD, that is, $V^{(b_3,b_4)}_{m,(b_2;k,l)} = U^{(b_3,b_4)}_{(b_2;k,l),m}$ and $\sigma^{(b_3,b_4)}_m$ can be negative. The truncation is performed in that case, taking the absolute values of $\{\sigma^{(b_3,b_4)}_m\}$ into consideration. In the case $b_3 = -b_4$, thanks to the reflection symmetry with respect to the $1'$-axis (see Appendix B), $M^{(b_3,b_4)}$ can be block diagonalized. To derive a block-diagonalized form, we introduce special indices O, A, B, O', A' and B',

$$O \in \{(0;i,j)|i = j\}, \tag{35}$$

$$A \in \{(0;i,j)|i > j\} \cup \{(b_1;i,j)|b_1 > 0\}, \tag{36}$$

$$B \in \{(0;i,j)|i < j\} \cup \{(b_1;i,j)|b_1 < 0\}, \tag{37}$$

$$O' \in \{(0;k,l)|k = l\}, \tag{38}$$

$$A' \in \{(0;k,l)|k > l\} \cup \{(b_2;k,l)|b_2 > 0\}, \tag{39}$$

$$B' \in \{(0;k,l)|k < l\} \cup \{(b_2;k,l)|b_2 < 0\}. \tag{40}$$

Then, $M^{(b_3,b_4)}$ is block diagonalized as follows:

$$
\begin{pmatrix} 1 & 0 & 0 \\ 0 & \frac{1}{\sqrt{2}} & \frac{(-1)^{p(i)+p(j)+b_1}}{\sqrt{2}} \\ 0 & \frac{1}{\sqrt{2}} & \frac{(-1)^{p(i)+p(j)+b_1+1}}{\sqrt{2}} \end{pmatrix}
\begin{pmatrix} M_{OO'} & M_{OA'} & M_{OB'} \\ M_{AO'} & M_{AA'} & M_{AB'} \\ M_{BO'} & M_{BA'} & M_{BB'} \end{pmatrix}
\begin{pmatrix} 1 & 0 & 0 \\ 0 & \frac{1}{\sqrt{2}} & \frac{1}{\sqrt{2}} \\ 0 & \frac{(-1)^{p(k)+p(l)+b_2}}{\sqrt{2}} & \frac{(-1)^{p(k)+p(l)+b_2+1}}{\sqrt{2}} \end{pmatrix}
$$

$$
= \begin{pmatrix} M_{OO'} & \sqrt{2}M_{OA'} & 0 \\ \sqrt{2}M_{AO'} & M_{AA'} + (-1)^{p(i)+p(j)+b_1}M_{BA'} & 0 \\ 0 & 0 & M_{AA'} - (-1)^{p(i)+p(j)+b_1}M_{BA'} \end{pmatrix}, \tag{41}
$$

where the superscript (b_3, b_4) is omitted. When b_3 is an odd (even) number, the upper-left (lower-right) block is parity odd under the reflection. If the index m that is introduced in the SVD, Eq. (34), is in the parity-odd block, $p(m) = 1$; otherwise $p(m) = 0$. By using the above result, we define a decomposition of the Grassmann-valued tensor $\mathcal{T}^{(b_1,b_2,b_3,b_4)}_n$ on even sites,

$$\mathcal{T}^{(b_1,b_2,b_3,b_4)}_{n;i,j,k,l} = \sum_{m,m'} \int \mathcal{S}^{1(b_3,b_4)}_{n^{(1)}+\hat{1}';(b_1;i,j),m'} \mathcal{S}^{3(b_3,b_4)}_{n^{(1)};(b_2;k,l),m} \mathcal{G}^{(1)(b_3,b_4)}_{n^{(1)},1';m',m}, \tag{42}$$

with

$$\mathcal{G}^{(1)(b_3,b_4)}_{n^{(1)},1';m',m} \equiv h^{(1)(b_3,b_4)}_{m',m} \xi^{R(b_3-b_4)+p(m)}_{n^{(1)},1} \bar{\xi}^{R(b_3-b_4)+p(m')}_{n^{(1)}+\hat{1}',1} \xi^{R(b_4-b_3)+p(m')}_{n^{(1)}+\hat{1}',2} \bar{\xi}^{R(b_4-b_3)+p(m)}_{n^{(1)},2}, \tag{43}$$

$$h^{(1)(b_3,b_4)}_{m',m} \equiv \operatorname{sgn}(\sigma^{(b_3,b_4)}_m) \delta_{m',m}, \tag{44}$$

$$\mathcal{S}^{1(b_3,b_4)}_{n^{(1)}+\hat{1}';(b_1;i,j),m'} \equiv S^{1(b_3,b_4)}_{(b_1;i,j),m'} d\bar{\xi}^{R(b_3-b_4)+p(m')}_{n^{(1)}+\hat{1}',1} d\xi^{R(b_4-b_3)+p(m')}_{n^{(1)}+\hat{1}',2} d\psi^{R(b_1-b_4)+p(i)}_{n,1} d\bar{\psi}^{R(b_4-b_1)+p(i)}_{n,2} d\bar{\chi}^{R(b_1-b_3)+p(j)}_{n,2} d\chi^{R(b_3-b_1)+p(j)}_{n,1}, \tag{45}$$

$$S^{1(b_3,b_4)}_{(b_1;i,j),m'} \equiv (-1)^{R(b_1-b_3)+R(b_1-b_4)+R(b_3-b_4)} \sqrt{|\sigma^{(b_3,b_4)}_{m'}|} V^{(b_4,b_3)}_{m',(b_1;i,j)}, \tag{46}$$

$$\mathcal{S}^{3(b_3,b_4)}_{n^{(1)};(b_2;k,l),m} \equiv S^{3(b_3,b_4)}_{(b_2;k,l),m} d\xi^{R(b_3-b_4)+p(m)}_{n^{(1)},1} d\bar{\xi}^{R(b_4-b_3)+p(m)}_{n^{(1)},2} d\bar{\psi}^{R(b_3-b_2)+p(k)}_{n,1} d\psi^{R(b_2-b_3)+p(k)}_{n,2} d\chi^{R(b_4-b_2)+p(l)}_{n,2} d\bar{\chi}^{R(b_2-b_4)+p(l)}_{n,1}, \quad (47)$$

$$S^{3(b_3,b_4)}_{(b_2;k,l),m} \equiv \sqrt{|\sigma^{(b_3,b_4)}_m|} V^{(b_3,b_4)}_{m,(b_2;k,l)}, \quad (48)$$

where sgn is a sign function and $\{\bar{\xi}_{n^{(1)}}, \xi_{n^{(1)}}\}$ are newly-introduced Grassmann variables with $n^{(1)}$ being a coarse-grained lattice site. This decomposition is schematically expressed in Fig. 2(a). It should be remarked that differently from our previous approach, $\xi_{n^{(1)}}$ is a two-component Grassmann variable and that is essential to preserve rotation and reflection symmetries. In Eq. (46), the π-rotation symmetry explained in Appendix B is employed and it is assumed that $\xi_{n^{(1)}}$ transforms under rotations as ψ_n does. A decomposition for odd sites is defined as follows by exploiting the rotation symmetry discussed in Appendix B:

$$\mathcal{T}^{(b_1,b_2,b_3,b_4)}_{n;i,j,k,l} = \sum_{m,m'} \int \mathcal{S}^{2(b_2,b_1)}_{n^{(1)}+\hat{2}';(b_3;j,k),m'} \mathcal{S}^{4(b_2,b_1)}_{n^{(1)};(b_4;l,i),m} \mathcal{G}^{(1)(b_2,b_1)}_{n^{(1)},2';m',m}, \quad (49)$$

with

$$\mathcal{G}^{(1)(b_2,b_1)}_{n^{(1)},2';m',m} \equiv h^{(1)(b_2,b_1)}_{m',m} \eta^{R(b_2-b_1)+p(m)}_{n^{(1)},1} \bar{\eta}^{R(b_2-b_1)+p(m')}_{n^{(1)}+\hat{2}',1} \eta^{R(b_1-b_2)+p(m')}_{n^{(1)}+\hat{2}',2} \bar{\eta}^{R(b_1-b_2)+p(m)}_{n^{(1)},2}, \quad (50)$$

$$\mathcal{S}^{2(b_2,b_1)}_{n^{(1)}+\hat{2}';(b_3;j,k),m'} \equiv S^{2(b_2,b_1)}_{(b_3;j,k),m'} d\eta^{R(b_1-b_2)+p(m')}_{n^{(1)}+\hat{2}',2} d\bar{\eta}^{R(b_2-b_1)+p(m')}_{n^{(1)}+\hat{2}',1} d\bar{\chi}^{R(b_1-b_3)+p(j)}_{n,2} d\chi^{R(b_3-b_1)+p(j)}_{n,1} d\bar{\psi}^{R(b_3-b_2)+p(k)}_{n,1} d\psi^{R(b_2-b_3)+p(k)}_{n,2},$$

$$\quad (51)$$

$$S^{2(b_2,b_1)}_{(b_3;j,k),m'} \equiv (-1)^{R(b_2-b_3)} \sqrt{|\sigma^{(b_2,b_1)}_{m'}|} V^{(b_1,b_2)}_{m',(b_3;j,k)}, \quad (52)$$

$$\mathcal{S}^{4(b_2,b_1)}_{n^{(1)};(b_4;l,i),m} \equiv S^{4(b_2,b_1)}_{(b_4;l,i),m} d\bar{\eta}^{R(b_1-b_2)+p(m)}_{n^{(1)},2} d\eta^{R(b_2-b_1)+p(m)}_{n^{(1)},1} d\chi^{R(b_4-b_2)+p(l)}_{n,2} d\bar{\chi}^{R(b_2-b_4)+p(l)}_{n,1} d\psi^{R(b_1-b_4)+p(i)}_{n,1} d\bar{\psi}^{R(b_4-b_1)+p(i)}_{n,2}, \quad (53)$$

$$S^{4(b_2,b_1)}_{(b_4;l,i),m} \equiv (-1)^{R(b_4-b_2)+R(b_1-b_2)} \sqrt{|\sigma^{(b_2,b_1)}_m|} V^{(b_2,b_1)}_{m,(b_4;l,i)}, \quad (54)$$

where $\{\bar{\eta}_{n^{(1)}}, \eta_{n^{(1)}}\}$ are also newly introduced Grassmann variables and transform under rotations as χ_n does. This decomposition is schematically expressed in Fig. 2(b).

Next, we perform a contraction for $\mathcal{S}^{1(b_3,b_2)}_{n^{(1)}}$, $\mathcal{S}^{2(b_3,b_1)}_{n^{(1)}}$, $\mathcal{S}^{3(b_1,b_4)}_{n^{(1)}}$ and $\mathcal{S}^{4(b_2,b_4)}_{n^{(1)}}$ as depicted in Fig. 3. The old Grassmann variables $\{\bar{\psi}_n, \psi_n, \bar{\xi}_n, \xi_n\}$ reside on a small closed loop in the figure and we can integrate out all of them simultaneously with the contraction. As a result, we get a coarse-grained tensor,

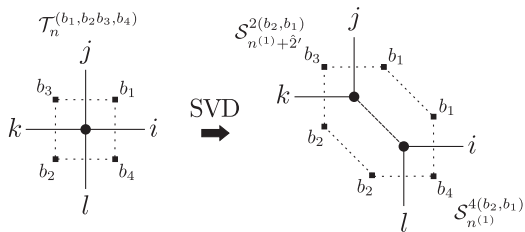(a) for even sites

(b) for odd sites

FIG. 2. Schematic representation for the decompositions of (a) Eq. (42) and (b) Eq. (49). Newly introduced Grassmann variables $\{\bar{\xi}_{n^{(1)}}, \xi_{n^{(1)}}, \bar{\eta}_{n^{(1)}}, \eta_{n^{(1)}}\}$ are assigned to the additional dashed lines.
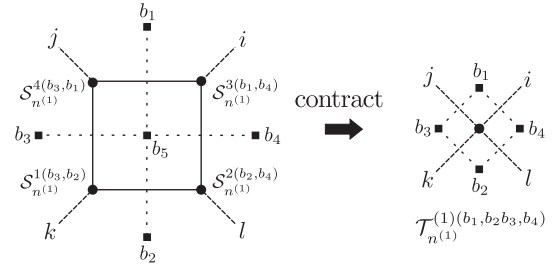

FIG. 3. Schematic representation of the contraction of Eq. (55). Solid lines in a closed loop, where old Grassmann variables $\{\bar{\psi}_n, \psi_n, \bar{\chi}_n, \chi_n\}$ reside, can be contracted and replaced by $\mathcal{T}^{(1)}_{n^{(1)}}$.

$$
\begin{aligned}
\mathcal{T}^{(1)(b_1,b_2,b_3,b_4)}_{n^{(1)};i,j,k,l} &= \sum_{b_5,p,q,r,s,p',q',r',s'} \int \mathcal{S}^{1(b_3,b_2)}_{n^{(1)};(b_5;p,q),k} \mathcal{S}^{2(b_2,b_4)}_{n^{(1)};(b_5;s,p'),l} \mathcal{S}^{3(b_1,b_4)}_{n^{(1)};(b_5;r',s'),i} \mathcal{S}^{4(b_3,b_1)}_{n^{(1)};(b_5;q',r),j} \\
&\quad \mathcal{G}^{(b_3,b_5)}_{n,2;q',q} \mathcal{G}^{(b_1,b_5)}_{n+\hat{2},1;r',r} \mathcal{G}^{(b_5,b_4)}_{n+\hat{1},2;s',s} \mathcal{G}^{(b_5,b_2)}_{n,1;p',p} \\
&= \sum_{b_5,p,q,r,s,p',q',r',s'} (-1)^{R(b_1-b_5)+R(b_2-b_5)+R(b_3-b_5)+R(b_4-b_5)+b_4+b_5} \\
&\quad \times S^{1(b_3,b_2)}_{(b_5;p,q),k} S^{2(b_2,b_4)}_{(b_5;s,p'),l} S^{3(b_1,b_4)}_{(b_5;r',s'),i} S^{4(b_3,b_1)}_{(b_5;q',r),j} h^{(b_3,b_5)}_{q',q} h^{(b_1,b_5)}_{r',r} h^{(b_5,b_4)}_{s',s} h^{(b_5,b_2)}_{p',p} \\
&\quad \times \mathrm{d}\xi^{R(b_1-b_4)+p(i)}_{n^{(1)},1} \mathrm{d}\bar{\xi}^{R(b_4-b_1)+p(i)}_{n^{(1)},2} \mathrm{d}\bar{\eta}^{R(b_1-b_3)+p(j)}_{n^{(1)},2} \mathrm{d}\eta^{R(b_3-b_1)+p(j)}_{n^{(1)},1} \\
&\quad \times \mathrm{d}\bar{\xi}^{R(b_3-b_2)+p(k)}_{n^{(1)},1} \mathrm{d}\xi^{R(b_2-b_3)+p(k)}_{n^{(1)},2} \mathrm{d}\eta^{R(b_4-b_2)+p(l)}_{n^{(1)},2} \mathrm{d}\bar{\eta}^{R(b_2-b_4)+p(l)}_{n^{(1)},1} \\
&\equiv T^{(1)(b_1,b_2,b_3,b_4)}_{i,j,k,l} \mathrm{d}\xi^{R(b_1-b_4)+p(i)}_{n^{(1)},1} \mathrm{d}\bar{\xi}^{R(b_4-b_1)+p(i)}_{n^{(1)},2} \mathrm{d}\bar{\eta}^{R(b_1-b_3)+p(j)}_{n^{(1)},2} \mathrm{d}\eta^{R(b_3-b_1)+p(j)}_{n^{(1)},1} \\
&\quad \times \mathrm{d}\bar{\xi}^{R(b_3-b_2)+p(k)}_{n^{(1)},1} \mathrm{d}\xi^{R(b_2-b_3)+p(k)}_{n^{(1)},2} \mathrm{d}\eta^{R(b_4-b_2)+p(l)}_{n^{(1)},2} \mathrm{d}\bar{\eta}^{R(b_2-b_4)+p(l)}_{n^{(1)},1},
\end{aligned}
\tag{55}
$$

where only the new Grassmann variables remain. It is easily confirmed that the constraints on the tensor kernel $T^{(1)(b_1,b_2,b_3,b_4)}$ from the rotation symmetry are the same as those on the initial tensor given in Appendix B. The constraints from the reflection symmetry are also derived by assuming appropriate transformality of $\xi_{n^{(1)}}$ and $\eta_{n^{(1)}}$. Roles of the 1-axis (2-axis) and $2'$-axis ($1'$-axis)

are swapped, compared with the case of the initial tensor.

Further iterations can be performed in a similar manner. After $N \equiv \log_2 L^2$ iterations with L being the lattice length, one N-times coarse-grained tensor $\mathcal{T}^{(N)(b_1,b_2,b_3,b_4)}_{n^{(N)}}$ covers whole lattice. Therefore, the density matrix ρ is represented as

$$
\begin{aligned}
\rho_{(b_1;i),(b_2;k)} &= \sum_{j,j',k'} \int \mathcal{T}^{(N)(b_1,b_2,b_2,b_1)}_{0;i,j,k',j'} \mathcal{G}^{(N)(b_2,b_2)}_{0,1;k',k} \mathcal{G}^{(N)(b_2,b_1)}_{0,2;j',j} \\
&= \sum_j (-1)^{R(b_2-b_1)} T^{(N)(b_1,b_2,b_2,b_1)}_{i,j,k,j} \mathrm{sgn}(\sigma^{(N-1)(b_2,b_2)}_k) \mathrm{sgn}(\sigma^{(N-1)(b_2,b_1)}_j),
\end{aligned}
\tag{56}
$$

and the partition function is $Z = \mathrm{tr}\rho$ where periodic boundary conditions are employed. The density matrix ρ can be block diagonalized because of the reflection symmetry with respect to the 1-axis, namely, the parity symmetry. That enables us to compute an expectation value of a projection operator into the parity-odd subspace as follows:

$$
\langle P_{\mathrm{odd}} \rangle = \frac{\mathrm{tr}(P_{\mathrm{odd}}\rho)}{Z} = \frac{1}{Z} \left\{ \left(\sum_{i:p(i)=1} \rho_{(0;i),(0;i)} \right) + \left[\sum_{b_1>0,i} \left(\rho_{(b_1;i),(b_1;i)} - (-1)^{p(i)} \rho_{(b_1;i),(-b_1;i)} \right) \right] \right\}.
\tag{57}
$$

Taking the large volume limit, it is one half in the parity-broken phase; otherwise it is 0.

III. NUMERICAL STUDY

A. Strong-coupling limit

Before investigation at finite couplings, we first examine the strong-coupling limit. In this case, the gauge action of Eq. (16) is dropped and the conventional TRG is applied rather than the decorated TRG as in Ref. [6]. Taking advantage of the symmetry-preserving algorithm, we calculate $\langle P_{\mathrm{odd}} \rangle$ according to Eq. (57) in order to detect a parity-broken phase in an explicit manner, while we employed the analyses of the Lee-Yang/Fisher zeros and

chiral susceptibility in Ref. [6]. Figure 4 shows our estimate of $\langle P_{\mathrm{odd}} \rangle$ on a $L = 2^{20}$ lattice with $D = 160$ as the SVD truncation parameter. It overtly indicates a parity-breaking transition around $m = -0.7$. We present the convergence behavior of $\langle P_{\mathrm{odd}} \rangle$ with increasing L around the transition point in Fig. 5. The D dependence of the transition point is given in Fig. 6, where good convergence is observed for $D \geq 80$ within the discretized resolution of $\Delta m = 0.00001$. We conclude that the critical mass is $m_c = -0.68648(1)$, which is consistent with values reported in Refs. [4,5] and also our previous result [6].

An important new finding is another phase transition around $m = -1.8$. It should be noted that this transition was not detected in our previous study using the chiral
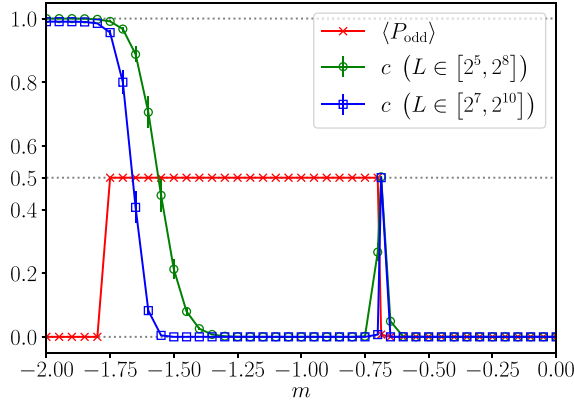
FIG. 4. $\langle P_{\mathrm{odd}} \rangle$ and central charge c as a function of fermion mass m at $g = \infty$ evaluated with $D = 160$. $\langle P_{\mathrm{odd}} \rangle$ is evaluated on a $L = 2^{20}$ lattice and c is from χ^2-fits with Eq. (59) for $L \in [2^5, 2^8]$ (circle) or $L \in [2^7, 2^{10}]$ (square). Dotted lines denote $\langle P_{\mathrm{odd}} \rangle = 0$, 0.5 and $c = 0$, 1 to guide eyes.

susceptibility analysis. One of the possible candidates is the Berezinskii-Kosterlitz-Thouless (BKT) transition, which does not have singularity in the free energy. To clarify the properties of the transition, we measure the central charge c, which should be 1 at the BKT criticality, one half at the Ising criticality, or 0 at noncriticality. As demonstrated by Gu and Wen using the TRG in Ref. [37], one can evaluate it from the largest eigenvalue of the density matrix ρ with the aid of CFT. Since the eigenvalues $\{\lambda_i\}$ are of a form

$$\lambda_i = e^{-f_\infty L^2 - 2\pi \left(\Delta_i - \frac{c}{12} \right)}, \qquad (58)$$

where f_∞ is a nonuniversal constant and $\{\Delta_i\}$ are scaling dimensions, we use the following equation for χ^2-fit:
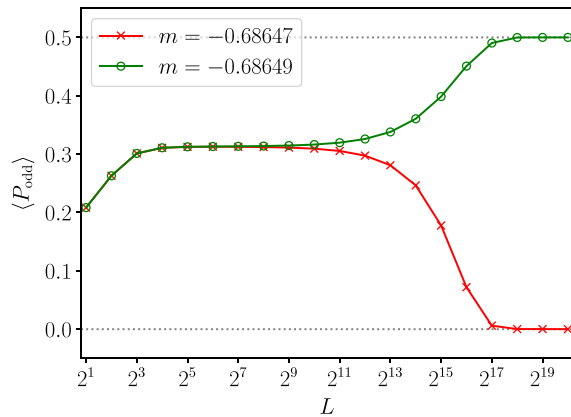

FIG. 5. Convergence of $\langle P_{\mathrm{odd}} \rangle$ at $g = \infty$ evaluated with $D = 160$ as a function of L. The result of $m = -0.68647$ goes to 0 (symmetric phase) while that of $m = -0.68649$ reaches one half (parity-broken phase). Dotted lines denote $\langle P_{\mathrm{odd}} \rangle = 0$, 0.5 to guide eyes.
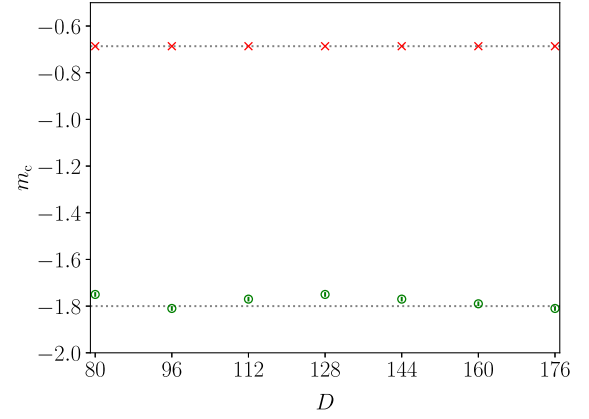

FIG. 6. Convergence of two phase transition points evaluated by a $\langle P_{\mathrm{odd}} \rangle$ analysis on a $L = 2^{20}$ lattice at $g = \infty$ as a function of the SVD truncation number D. Dotted lines are for guiding eyes.

$$\ln \lambda_0 = \frac{\pi c}{6} - f_\infty L^2. \qquad (59)$$

Note that our algorithm given in Sec. II does not preserve hermiticity of the density matrix and it is numerically broken. Because of this, we instead compute singular values as our estimate of eigenvalues. Figure 7 shows L dependence of the largest eigenvalue λ_0 at $m = -1.79$, -0.68648, whose errors are estimated by the difference between the results with $D = 160$ and 80, and Table I summarizes the fit results, which indicate $c = 1$ for $m = -1.79$ and $c = \frac{1}{2}$ for $m = -0.68648$. The m dependence of the central charge is plotted in Fig. 4. We observe a wide range of $c = 1$ for $m \lesssim -1.8$, while a clear $c = \frac{1}{2}$ peak is found around $m = -0.7$ of the Ising transition point. The existence of the critical region (not point) for $m \lesssim -1.8$ is consistent with an expected property of the BKT transition. Note that the central charge in Fig. 4 rises up more gently than $\langle P_{\mathrm{odd}} \rangle$. One of the main reasons is that the central
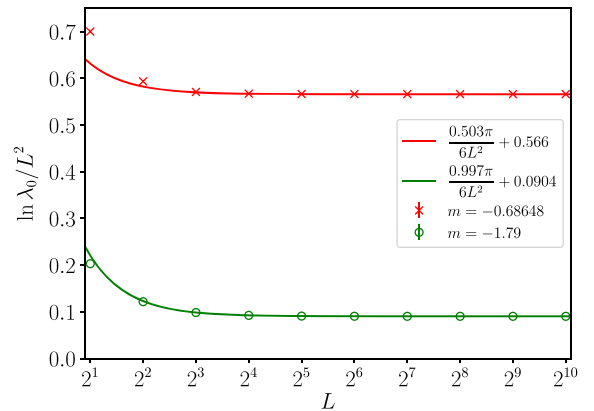

FIG. 7. The largest eigenvalue λ_0 of the density matrix ρ at $g = \infty$ evaluated with $D = 160$ as a function of L. Two cases of $m = -0.68648$ and $m = -1.79$ are presented. Solid curves represent fit results with Eq. (59) for $L \in [2^5, 2^8]$.

TABLE I. Fit results of λ_0 with Eq. (59) at $g = \infty$ for $L \in [2^5, 2^8]$. λ_0 is evaluated with $D = 160$.

m	c	f_∞	$\sqrt{\chi^2/\text{d.o.f}}$
-0.68648	$0.50272(30)$	$-0.566320061(79)$	4.5
-1.79	$0.99668(99)$	$-0.09038590(23)$	0.035

charge is estimated with data sets of somewhat smaller lattices in order to avoid accumulation of the SVD truncation error that makes the TRG flows go away from the critical surface. The finite size effect is clearly observed by comparing two fit results between $L \in [2^5, 2^8]$ and $L \in [2^7, 2^{10}]$. On the other hand, $\langle P_{\text{odd}} \rangle$ is a quantity related to a rather trivial fixed point that renormalization group flows finally reach away from criticality. It is less contaminated by the SVD truncation error so that we are allowed to take the large L limit more reliably. However, it should be noted that $\langle P_{\text{odd}} \rangle$ is much more unstable around the BKT transition point than the Ising transition point: Our estimate of the BKT transition point by the $\langle P_{\text{odd}} \rangle$ analysis has larger D dependence as observed in Fig. 6.

We also measure scaling dimensions using Eq. (58),

$$\Delta_i = \frac{1}{2\pi} \ln\left(\frac{\lambda_0}{\lambda_i}\right). \quad (60)$$

In a BKT phase, $\{\Delta_i\}$ vary continuously due to the existence of an exactly marginal operator. At $m = -2$ the model is mapped to a critical six-vertex model that belongs to a universality class described by a free boson compactified on a circle with radius $R = \frac{1}{\sqrt{2}}$ (see, e.g., Ref. [38]). In this case, the scaling dimensions are known to be

$$\Delta_i = \frac{M^2}{4R^2} + R^2 N^2, \qquad M, N \in \mathbb{Z}, \quad (61)$$

which means that all the lowest four nonzero scaling dimensions Δ_1, Δ_2, Δ_3 and Δ_4 are equal to one half. The top panel of Fig. 8 shows L dependence of the scaling dimensions. We find sizable deviation from one half, especially for Δ_4, compared to the case of $(m, g) = (-0.68648, \infty)$ in Fig. 9, where $\Delta_1 = \frac{1}{8}$, $\Delta_2 = 1$ and $\Delta_3 = \Delta_4 = \frac{9}{8}$ is expected for the Ising transition. This is due to the well-known fact that the existence of an exactly marginal operator in the BKT transition causes a universal $\mathcal{O}((\ln L)^{-1})$ correction to the scaling dimensions while the central charge is affected by a smaller correction of $\mathcal{O}((\ln L)^{-3})$ [39,40]. Although precise determination of the scaling dimensions requires much larger lattice size, accumulation of the SVD truncation error makes it difficult (see D dependence of the scaling dimensions evaluated at $L = 2^{10}$ in the bottom panel of Fig. 8).

Putting aside the logarithmic finite size corrections on the scaling dimensions, it should be important to point out
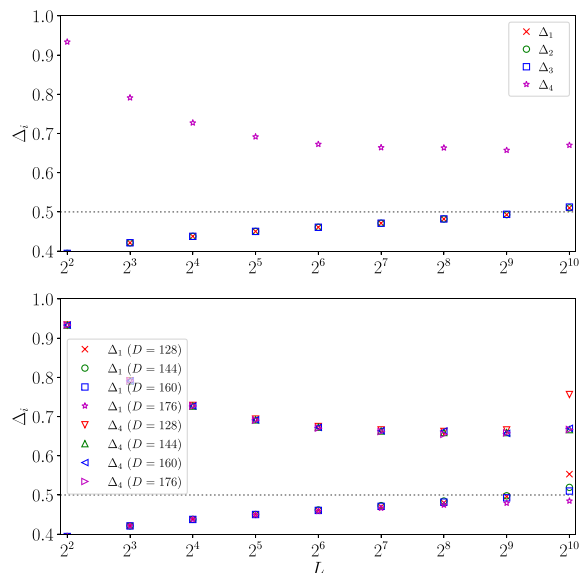

FIG. 8. Top: scaling dimensions Δ_1, Δ_2, Δ_3 and Δ_4 at $(m, g) = (-2, \infty)$ as a function of L evaluated with $D = 160$. The dotted line denotes $\Delta_i = 0.5$ to guide eyes. Bottom: D dependence of Δ_1 and Δ_4. The dotted line denotes $\Delta_i = 0.5$ to guide eyes.

that Δ_1, Δ_2, and Δ_3 form a triplet. The free boson compactified with $R = \frac{1}{\sqrt{2}}$ corresponds to a CFT with an SU(2) symmetry and the triplet spectrum is ascribed to it. Note that the $S = \frac{1}{2}$ Heisenberg XXX model belongs to the same universality class and its scaling dimensions obtained by numerically solving the Bethe ansatz equations show similar behavior to our result [41,42]: the triplet spectrum close to the value of one half and the singlet one deviated from the value of one half. A remaining question of interest is whether or not the SU(2) symmetry arises at $m = -2$ only. We present m dependence of the scaling dimensions in the BKT phase around $m = -2$ in Fig. 10, where we find that the triplet spectrum is observed only at $m = -2$.
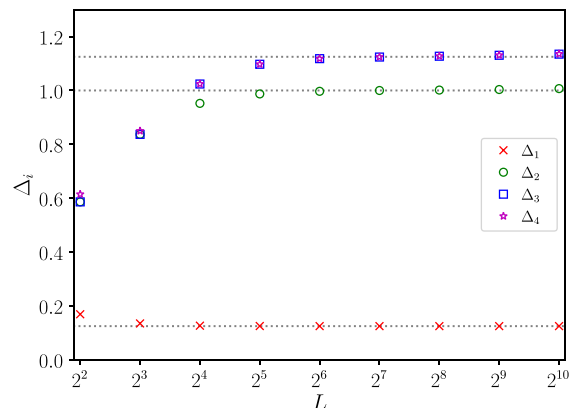

FIG. 9. Scaling dimensions Δ_1, Δ_2, Δ_3 and Δ_4 at $(m, g) = (-0.68648, \infty)$ as a function of L evaluated with $D = 160$. The dotted lines denote $\Delta_1 = \frac{1}{8}$, $\Delta_2 = 1$ and $\Delta_3 = \Delta_4 = \frac{9}{8}$ to guide eyes.
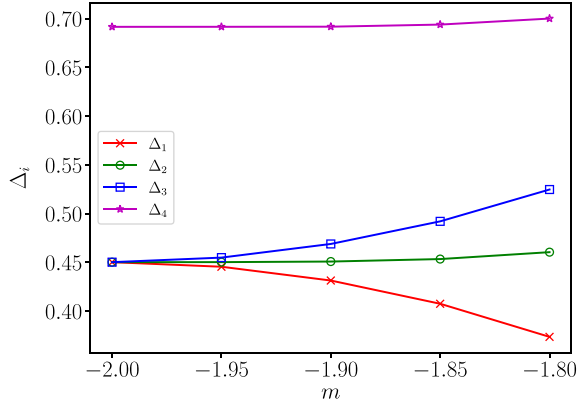
FIG. 10. Scaling dimensions Δ_1, Δ_2, Δ_3 and Δ_4 at $g = \infty$ evaluated with $D = 160$ on a $L = 2^5$ lattice as a function of m in the BKT phase.

B. Finite couplings

We employ three couplings $g = 1.0$, 0.5, 0.1 to investigate the phase structure in the finite-coupling region, where an additional parameter N_{ce} is required to control the truncation of the character expansion. In our previous approach with the conventional TRG method in Refs. [6,13], only the initial tensor size is related to the truncation number N_{ce} and we chose a somewhat excessive value to safely neglect the truncation error. However, the computational cost of the decorated TRG method heavily depends on N_{ce} and smaller values are preferred. Figure 11 shows our estimate of Δ_1 at $(m, g) = (-2, 0.1)$ with several values of N_{ce}. The result looks converged for $N_{ce} \geq 3$ even on smaller lattices so that we employ $N_{ce} = 3$ in this work. Since the convergency property of the character expansion becomes better toward the strong-coupling limit, the choice of $N_{ce} \geq 3$ is also valid for the cases of $g = 1.0$, 0.5. It should be noted that our choice of the SVD truncation number D in the finite-coupling study is much smaller than in the case of the strong-coupling limit with the
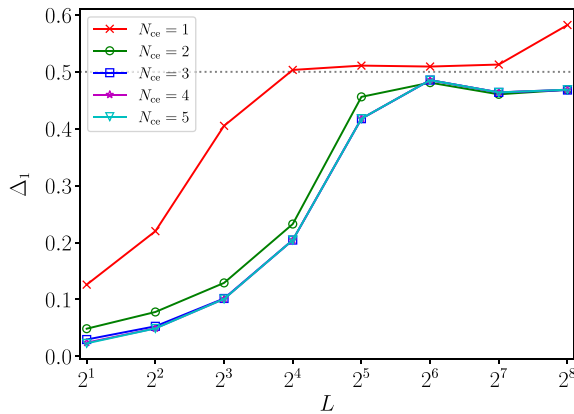

FIG. 11. The lowest nonzero scaling dimension Δ_1 evaluated at $(m, g) = (-2, 0.1)$ with $D = 48$ and $N_{ce} = 1, \ldots, 5$ as a function of L. The dotted line denotes $\Delta_1 = 0.5$ to guide eyes.
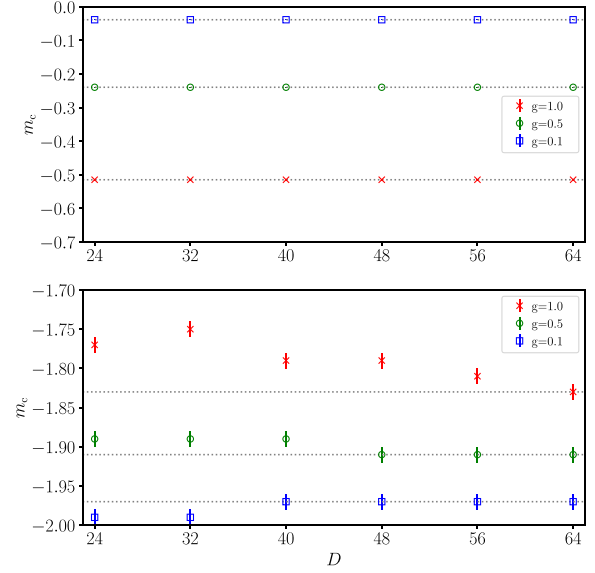

FIG. 12. Convergence behavior of the Ising transition point (top) and the BKT transition point (bottom) as a function of the SVD truncation number D. $\langle P_{odd} \rangle$ analysis is made at $g = 1.0$, 0.5, 0.1 on a $L = 2^{20}$ lattice with $N_{ce} = 3$. The dotted lines are for guiding eyes.
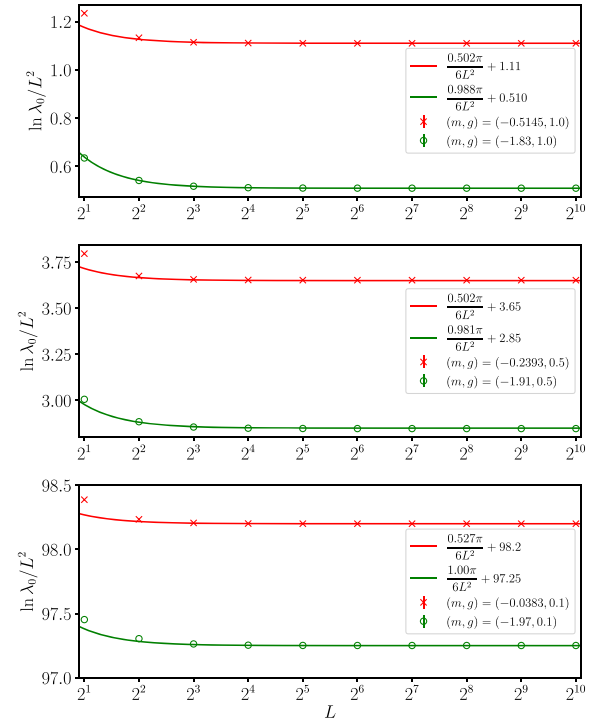

FIG. 13. The largest eigenvalue λ_0 of the density matrix ρ evaluated at $g = 1.0$, 0.5, 0.1 (from top to bottom) with $D = 64$ and $N_{ce} = 3$ as a function of L. Both cases of the Ising (red) and BKT (green) transitions are presented. Solid curves represent fit results with Eq. (59) for $L \in [2^5, 2^8]$.

TABLE II. Fit results of λ_0 with Eq. (59) at finite couplings for $L \in [2^5, 2^8]$. λ_0 is evaluated with $D = 64$ and $N_{ce} = 3$.

g	m	c	f_∞	$\sqrt{\chi^2/\mathrm{d.o.f}}$
1.0	−0.5145	0.50170(22)	−1.109792127(56)	0.054
1.0	−1.83	0.98785(74)	−0.51022075(18)	0.0033
0.5	−0.2393	0.50169(21)	−3.652315026(54)	0.037
0.5	−1.91	0.9805(25)	−2.84754415(61)	0.0093
0.1	−0.0383	0.5270(37)	−98.20031257(84)	0.59
0.1	−1.97	0.999(24)	−97.2509086(61)	0.052

conventional TRG method. In the case of the decorated TRG method, however, we eventually take $D \times (2N_{ce}+1)^2$ singular values overall with the choice of D singular values in each block.

Carrying out the same analyses as the strong-coupling limit, we find two phase transition points at finite couplings. Figure 12 plots the values of m_c at these transition points as a function of D, which are determined by the $\langle P_{odd} \rangle$ analysis. Figure 13 shows L dependence of the largest eigenvalue of the density matrix ρ at the transition points, whose errors are estimated by the difference between the results with $D = 64$ and 32. The fit with Eq. (59) gives the central charge listed in Table II. These results clearly show that two transitions at each coupling are the Ising and BKT types and the former moves to $m = 0$ and the latter to $m = -2$ toward the weak-coupling limit.
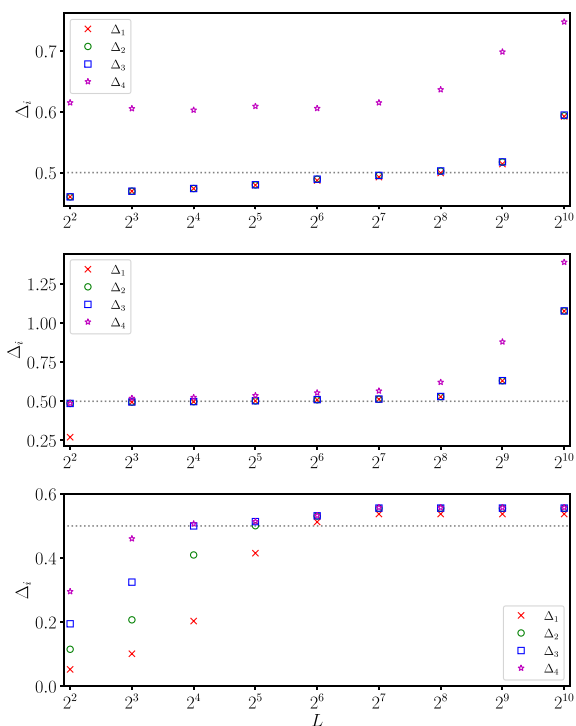

FIG. 14. Scaling dimensions Δ_1, Δ_2, Δ_3, and Δ_4 evaluated at $(m, g) = (-2, 1.0)$ (top), $(-2, 0.5)$ (middle), and $(-2, 0.1)$ (bottom) with $D = 64$ and $N_{ce} = 3$ as a function of L. The dotted line denotes $\Delta_i = 0.5$ to guide eyes.
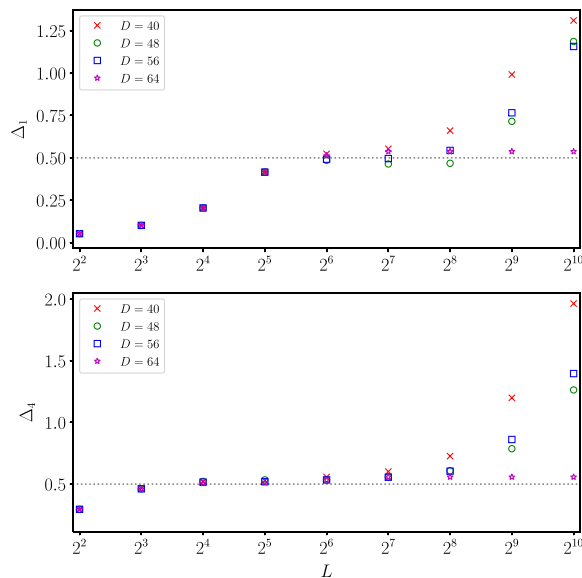

FIG. 15. D dependence of scaling dimensions Δ_1 (top) and Δ_4 (bottom) evaluated at $(m, g) = (-2, 0.1)$ with $N_{ce} = 3$ as a function of L. Dotted lines denote $\Delta_1 = \Delta_4 = 0.5$ to guide eyes.

One may expect that the SU(2) symmetry arises at $m = -2$ even in finite-coupling cases. We present our estimate of the scaling dimensions Δ_1, Δ_2, Δ_3, and Δ_4 at $m = -2$ as a function of L in Fig. 14. The triplet spectrum is observed in all the cases, though our results are rather contaminated by the SVD truncation error (see Fig. 15 for D dependence of the scaling dimensions).

From the above investigations, we determine the phase structure of the lattice Schwinger model with one flavor of the Wilson fermion as depicted in Fig. 16. The reflection symmetry of the Wilson fermion with respect to the $m = -2$ axis is exploited in the figure. One of the characteristic features different from the Aoki phase is that only one
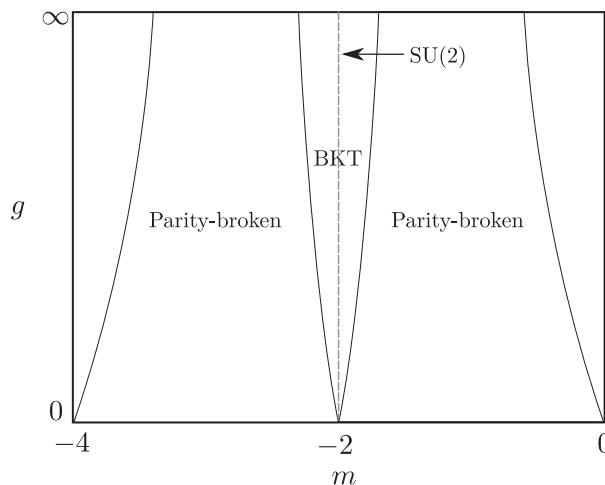

FIG. 16. Phase diagram of the lattice Schwinger model with one flavor of the Wilson fermion based on our analyses.

transition line arises from $(m, g) = (0, 0)$ [and $(m, g) = (-4, 0)$]. The same structure is reported in Ref. [43] where the lattice Gross-Neveu model with one flavor of the Wilson fermion was studied using a method based on the weak-coupling expansion.

IV. SUMMARY AND OUTLOOK

We have performed a detailed study of the phase structure of the lattice Schwinger model with one flavor of the Wilson fermion by developing a decorated Grassmann TRG method. By implementing an algorithm that preserves the reflection symmetry, we are allowed to evaluate an expectation value of a projection operator into the parity-odd subspace, which reveals a parity-broken phase in a clear manner. We have found not only an Ising phase transition, which was already known in our previous study, but also a BKT phase transition both in the strong-coupling limit and the finite-coupling region by measuring the central charge. Furthermore, our analysis of the scaling dimensions has shown that a CFT with the SU(2) symmetry arises at $(m, g) = (-2, \infty)$, where the lattice Schwinger model is known to be equivalent to a critical six-vertex model, and is retained along the line of $m = -2$ in the finite-coupling region of the (m, g) plane.

There is a numerical difficulty of accumulation of the SVD truncation error in the study of the BKT phase. The scaling dimensions suffer from a logarithmic finite size correction, which hinders us from quantitative understanding of the properties of the BKT phase at a high level of precision. In recent years, however, the TRG method has been improved rapidly [44–48]. These methods allow us to reach larger lattices with higher accuracy even at criticality. Further development would open a new path to precise numerical studies of the BKT transition.

It should be noted that the phase structure of the lattice Schwinger model with two or more flavors of the Wilson fermion is also of great interest. The Mermin-Wagner theorem prohibits the parity-flavor breaking for finite numbers of flavors but massless pseudoscalar mesons appear in the continuum Schwinger model. Extending our method to multiflavor cases is straightforward in principle. However, an efficient way to control the increasing degrees of freedom due to the multiflavor would be indispensable for practical numerical computation.

APPENDIX A: DETAIL OF THE INITIAL TENSOR

We list all the nonzero components of the decorated tensor kernel $T^{(b_1, b_2, b_3, b_4)}$ introduced in Eq. (29). Here it is useful to classify $T^{(b_1, b_2, b_3, b_4)}$ into 19 cases according to the decoration labels b_1, b_2, b_3, and b_4. The following abbreviation is used for simplicity:

$$I_{b_1, b_2, b_3, b_4} \equiv \left[I_{b_1}\left(\frac{1}{g}\right) I_{b_2}\left(\frac{1}{g}\right) I_{b_3}\left(\frac{1}{g}\right) I_{b_4}\left(\frac{1}{g}\right) \right]^{\frac{1}{4}}. \quad (A1)$$

For each tensor index, the value of 1 (2) corresponds to a parity-even (-odd) state, namely, $p(1) = 0$ and $p(2) = 1$. Symmetry of the tensor is discussed in Appendix B.

1. $b_1 - b_4 = b_3 - b_1 = b_3 - b_2 = b_2 - b_4 = 0$

The dimension of all tensor indices is 2 in this case. The nonzero components are as follows:

$$T^{(b_1, b_2, b_3, b_4)}_{1,1,1,1} = (m + 2)^2 I_{b_1, b_2, b_3, b_4},$$

$$T^{(b_1, b_2, b_3, b_4)}_{2,1,2,1} = T^{(b_1, b_2, b_3, b_4)}_{1,2,1,2} = I_{b_1, b_2, b_3, b_4},$$

$$T^{(b_1, b_2, b_3, b_4)}_{2,2,1,1} = T^{(b_1, b_2, b_3, b_4)}_{1,2,2,1} = T^{(b_1, b_2, b_3, b_4)}_{1,1,2,2}$$

$$= T^{(b_1, b_2, b_3, b_4)}_{2,1,1,2} = \frac{1}{2} I_{b_1, b_2, b_3, b_4}.$$

2. $b_1 - b_4 = b_3 - b_2 = 1$ and $b_3 - b_1 = b_2 - b_4 = 0$

The dimension of the first and third tensor indices is 1. That of the second and fourth ones is 2. The nonzero components are as follows:

$$T^{(b_1, b_2, b_3, b_4)}_{1,1,1,1} = (m + 2) I_{b_1, b_2, b_3, b_4},$$

$$T^{(b_1, b_2, b_3, b_4)}_{1,2,1,1} = -T^{(b_1, b_2, b_3, b_4)}_{1,1,1,2} = \frac{1}{2} I_{b_1, b_2, b_3, b_4}.$$

3. $b_1 - b_4 = b_3 - b_2 = 0$ and $b_3 - b_1 = b_2 - b_4 = 1$

This case is given by a $\frac{\pi}{2}$ rotation of the case A 2.

4. $b_1 - b_4 = b_3 - b_2 = -1$ and $b_3 - b_1 = b_2 - b_4 = 0$

This case is given by a π rotation of the case A 2.

5. $b_1 - b_4 = b_3 - b_2 = 0$ and $b_3 - b_1 = b_2 - b_4 = -1$

This case is given by a $-\frac{\pi}{2}$ rotation of the case A 2.

6. $b_1 - b_4 = 1$, $b_3 - b_1 = -1$ and $b_3 - b_2 = b_2 - b_4 = 0$

The dimension of the first and second tensor indices is 1. That of the third and fourth ones is 2. The nonzero components are as follows:

$$T^{(b_1,b_2,b_3,b_4)}_{1,1,1,1} = \frac{m+2}{\sqrt{2}} I_{b_1,b_2,b_3,b_4},$$

$$T^{(b_1,b_2,b_3,b_4)}_{1,1,2,1} = T^{(b_1,b_2,b_3,b_4)}_{1,1,1,2} = -\frac{1}{\sqrt{2}} I_{b_1,b_2,b_3,b_4}.$$

7. $b_1 - b_4 = b_2 - b_4 = 0$ and $b_3 - b_1 = b_3 - b_2 = 1$

This case is given by a $\frac{\pi}{2}$ rotation of the case A 6.

8. $b_1 - b_4 = b_3 - b_1 = 0$, $b_3 - b_2 = -1$ and $b_2 - b_4 = 1$

This case is given by a π rotation of the case A 6.

9. $b_1 - b_4 = b_2 - b_4 = -1$ and $b_3 - b_1 = b_3 - b_2 = 0$

This case is given by a $-\frac{\pi}{2}$ rotation of the case A 6.

10. $b_1 - b_4 = -1$, $b_3 - b_1 = 1$ and $b_3 - b_2 = b_2 - b_4 = 0$

This case is given by a reflection with respect to the $1'$-axis (see Fig. 17) of the case A 6.

11. $b_1 - b_4 = b_2 - b_4 = 0$ and $b_3 - b_1 = b_3 - b_2 = -1$

This case is given by a reflection with respect to the 2-axis (see Fig. 17) of the case A 6.

12. $b_1 - b_4 = b_3 - b_1 = 0$, $b_3 - b_2 = 1$ and $b_2 - b_4 = -1$

This case is given by a reflection with respect to the $2'$-axis (see Fig. 17) of the case A 6.

13. $b_1 - b_4 = b_2 - b_4 = 1$ and $b_3 - b_1 = b_3 - b_2 = 0$

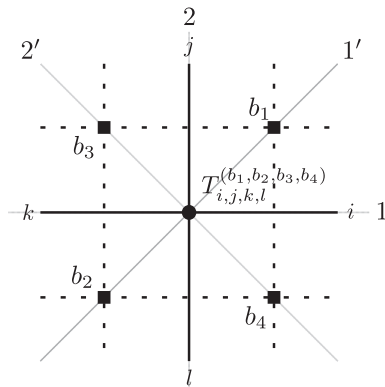This case is given by a reflection with respect to the 1-axis (see Fig. 17) of the case A 6.

FIG. 17. Definition of the 1-, 2-, $1'$- and $2'$-axes.

14. $b_1 - b_4 = b_3 - b_1 = b_3 - b_2 = b_2 - b_4 = 1$

The dimension of all tensor indices is 1 in this case. Therefore, the tensor has only one component,

$$T^{(b_1,b_2,b_3,b_4)}_{1,1,1,1} = -\frac{1}{2} I_{b_1,b_2,b_3,b_4}.$$

15. $b_1 - b_4 = b_3 - b_2 = -1$ and $b_3 - b_1 = b_2 - b_4 = 1$

This case is given by a $\frac{\pi}{2}$ rotation of the case A 14.

16. $b_1 - b_4 = b_3 - b_1 = b_3 - b_2 = b_2 - b_4 = -1$

This case is given by a π rotation of the case A 14.

17. $b_1 - b_4 = b_3 - b_2 = 1$ and $b_3 - b_1 = b_2 - b_4 = -1$

This case is given by a $-\frac{\pi}{2}$ rotation of the case A 14.

18. $b_1 - b_4 = b_2 - b_4 = 1$ and $b_3 - b_1 = b_3 - b_2 = -1$

The dimension of all tensor indices is 1 in this case. Therefore, the tensor has only one component,

$$T^{(b_1,b_2,b_3,b_4)}_{1,1,1,1} = I_{b_1,b_2,b_3,b_4}.$$

19. $b_1 - b_4 = b_2 - b_4 = -1$ and $b_3 - b_1 = b_3 - b_2 = 1$

This case is given by a $\frac{\pi}{2}$ rotation of the case A 18.

APPENDIX B: ROTATION AND REFLECTION SYMMETRIES

Discrete rotation and reflection symmetries in the lattice action bring some constraints on each tensor in the decorated tensor network of Eq. (28). First, we discuss the discrete rotation symmetry. Under a $\frac{\pi}{2}$ rotation, the Grassmann variables ψ_n, χ_n and the decoration labels $\{b_i\}$ transform as

$$\begin{pmatrix} \psi_{n,1} \\ \psi_{n,2} \end{pmatrix} \to \pm \begin{pmatrix} \cos\frac{\pi}{4} & \sin\frac{\pi}{4} \\ -\sin\frac{\pi}{4} & \cos\frac{\pi}{4} \end{pmatrix} \begin{pmatrix} \psi_{n,1} \\ \psi_{n,2} \end{pmatrix}$$

$$= \pm \begin{pmatrix} \chi_{n,1} \\ -\chi_{n,2} \end{pmatrix}, \tag{B1}$$

$$\begin{pmatrix} \chi_{n,1} \\ \chi_{n,2} \end{pmatrix} \to \pm \begin{pmatrix} \psi_{n,2} \\ \psi_{n,1} \end{pmatrix}, \tag{B2}$$

$$(b_1, b_2, b_3, b_4) \to (b_4, b_3, b_1, b_2), \tag{B3}$$

where a couple of signs for the Grassmann variables stem from the fact that they transform according to a two-valued representation of the rotation group. Then, we get the following constraint by imposing the $\frac{\pi}{2}$-rotation symmetry on each tensor:

$$T_{l,i,j,k}^{(b_4,b_3,b_1,b_2)} = (-1)^{R(b_4-b_1)+R(b_2-b_3)+b_2+b_4}$$
$$\times T_{i,j,k,l}^{(b_1,b_2,b_3,b_4)}. \tag{B4}$$

Similarly, other constraints from the π- and $-\frac{\pi}{2}$-rotation symmetry are obtained,

$$T_{k,l,i,j}^{(b_2,b_1,b_4,b_3)} = (-1)^{R(b_4-b_1)+R(b_3-b_1)+R(b_2-b_3)+R(b_2-b_4)}$$
$$\times (-1)^{b_3+b_4} T_{i,j,k,l}^{(b_1,b_2,b_3,b_4)}, \tag{B5}$$

$$T_{j,k,l,i}^{(b_3,b_4,b_2,b_1)} = (-1)^{R(b_1-b_3)+R(b_4-b_2)+b_1+b_4}$$
$$\times T_{i,j,k,l}^{(b_1,b_2,b_3,b_4)}. \tag{B6}$$

Next, let us turn to the reflection symmetry. Under a reflection with respect to the 1-axis (see Fig. 17), namely, space inversion, ψ_n, χ_n, and $\{b_i\}$ transform as

$$\begin{pmatrix} \psi_{n,1} \\ \psi_{n,2} \end{pmatrix} \to \gamma_1 \begin{pmatrix} \psi_{n,1} \\ \psi_{n,2} \end{pmatrix} = \begin{pmatrix} \psi_{n,1} \\ -\psi_{n,2} \end{pmatrix}, \tag{B7}$$

$$\begin{pmatrix} \chi_{n,1} \\ \chi_{n,2} \end{pmatrix} \to \begin{pmatrix} \chi_{n,2} \\ \chi_{n,1} \end{pmatrix}, \tag{B8}$$

$$(b_1, b_2, b_3, b_4) \to (-b_4, -b_3, -b_2, -b_1). \tag{B9}$$

Symmetry under these transformations brings

$$T_{i,l,k,j}^{(-b_4,-b_3,-b_2,-b_1)} = (-1)^{R(b_4-b_1)+R(b_2-b_3)}$$
$$\times (-1)^{(b_1+b_3)(b_2+b_3)+(b_1+b_2)(b_2+b_4)}$$
$$\times (-1)^{p(i)+p(j)+p(k)+p(l)} T_{i,j,k,l}^{(b_1,b_2,b_3,b_4)}. \tag{B10}$$

Transformation under a reflection with respect to the 2-axis (see Fig. 17), namely, time inversion is analogous,

$$\begin{pmatrix} \psi_{n,1} \\ \psi_{n,2} \end{pmatrix} \to \gamma_2 \begin{pmatrix} \psi_{n,1} \\ \psi_{n,2} \end{pmatrix} = \begin{pmatrix} \psi_{n,2} \\ \psi_{n,1} \end{pmatrix}, \tag{B11}$$

$$\begin{pmatrix} \chi_{n,1} \\ \chi_{n,2} \end{pmatrix} \to \begin{pmatrix} \chi_{n,1} \\ -\chi_{n,2} \end{pmatrix}, \tag{B12}$$

$$(b_1, b_2, b_3, b_4) \to (-b_3, -b_4, -b_1, -b_2), \tag{B13}$$

and a derived constraint is

$$T_{k,j,i,l}^{(-b_3,-b_4,-b_1,-b_2)} = (-1)^{R(b_1-b_3)+R(b_4-b_2)}$$
$$\times (-1)^{(b_1+b_3)(b_1+b_4)+(b_2+b_3)(b_3+b_4)}$$
$$\times (-1)^{p(i)+p(j)+p(k)+p(l)} T_{i,j,k,l}^{(b_1,b_2,b_3,b_4)}. \tag{B14}$$

We consider reflections with respect to the 1′- and 2′-axes also, which are defined in Fig. 17. That with respect to the 1′-axis is interpreted as a $\frac{\pi}{2}$ rotation followed by a reflection with respect to the 1-axis. The other is a $-\frac{\pi}{2}$ rotation followed by a reflection with respect to the 1-axis. Thus, the following constraints are obtained:

$$T_{j,i,l,k}^{(-b_1,-b_2,-b_4,-b_3)}$$
$$= (-1)^{(b_1+b_3)(b_1+b_4)+(b_2+b_3)(b_2+b_4)}$$
$$\times (-1)^{p(i)+p(j)+p(k)+p(l)} T_{i,j,k,l}^{(b_1,b_2,b_3,b_4)}, \tag{B15}$$

$$T_{l,k,j,i}^{(-b_2,-b_1,-b_3,-b_4)}$$
$$= (-1)^{R(b_1-b_4)+R(b_1-b_3)+R(b_3-b_2)+R(b_4-b_2)}$$
$$\times (-1)^{(b_1+b_3)(b_1+b_4)+(b_2+b_3)(b_2+b_4)+b_3+b_4}$$
$$\times (-1)^{p(i)+p(j)+p(k)+p(l)} T_{i,j,k,l}^{(b_1,b_2,b_3,b_4)}. \tag{B16}$$

[1] S. Aoki, Nucl. Phys. **B314**, 79 (1989).
[2] C. Vafa and E. Witten, Phys. Rev. Lett. **53**, 535 (1984).
[3] S. Aoki, M. Fukugita, S. Hashimoto, K.-I. Ishikawa, N. Ishizuka, Y. Iwasaki, K. Kanaya, T. Kaneko, Y. Kuramashi, M. Okawa, N. Tsutsui, A. Ukawa, N. Yamada, and T. Yoshié, Phys. Rev. D **72**, 054510 (2005).
[4] H. Gausterer and C. Lang, Nucl. Phys. **B455**, 785 (1995).
[5] U. Wenger, Phys. Rev. D **80**, 071503 (2009).
[6] Y. Shimizu and Y. Kuramashi, Phys. Rev. D **90**, 014508 (2014).
[7] M. Salmhofer, Nucl. Phys. **B362**, 641 (1991).
[8] M. Levin and C. P. Nave, Phys. Rev. Lett. **99**, 120601 (2007).
[9] Y. Shimizu, Mod. Phys. Lett. A **27**, 1250035 (2012).
[10] Y. Liu, Y. Meurice, M. P. Qin, J. Unmuth-Yockey, T. Xiang, Z. Y. Xie, J. F. Yu, and H. Zou, Phys. Rev. D **88**, 056005 (2013).
[11] A. Denbleyker, Y. Liu, Y. Meurice, M. P. Qin, T. Xiang, Z. Y. Xie, J. F. Yu, and H. Zou, Phys. Rev. D **89**, 016008 (2014).
[12] H. Zou, Y. Liu, C.-Y. Lai, J. Unmuth-Yockey, L.-P. Yang, A. Bazavov, Z. Y. Xie, T. Xiang, S. Chandrasekharan, S.-W. Tsai, and Y. Meurice, Phys. Rev. A **90**, 063603 (2014).

[13] Y. Shimizu and Y. Kuramashi, Phys. Rev. D **90**, 074503 (2014).

[14] B. Dittrich, S. Mizera, and S. Steinhaus, New J. Phys. **18**, 053009 (2016).

[15] S. Takeda and Y. Yoshimura, Prog. Theor. Exp. Phys. **2015**, 043B01 (2015).

[16] A. Bazavov, Y. Meurice, S.-W. Tsai, J. Unmuth-Yockey, and J. Zhang, Phys. Rev. D **92**, 076003 (2015).

[17] H. Kawauchi and S. Takeda, Phys. Rev. D **93**, 114503 (2016).

[18] A. Bazavov, Y. Meurice, S. W. Tsai, J. Unmuth-Yockey, L.-P. Yang, and J. Zhang, Phys. Rev. D **96**, 034514 (2017).

[19] R. Sakai, S. Takeda, and Y. Yoshimura, Prog. Theor. Exp. Phys. **2017**, 063B07 (2017).

[20] Y. Yoshimura, Y. Kuramashi, Y. Nakamura, S. Takeda, and R. Sakai, arXiv:1711.08121.

[21] C. Delcamp and B. Dittrich, Classical Quantum Gravity **34**, 225006 (2017).

[22] Z.-C. Gu, F. Verstraete, and X.-G. Wen, arXiv:1004.2563.

[23] T. M. R. Byrnes, P. Sriganesh, R. J. Bursill, and C. J. Hamer, Phys. Rev. D **66**, 013002 (2002).

[24] M. C. Bañuls, K. Cichy, K. Jansen, and J. I. Cirac, J. High Energy Phys. 11 (2013) 158.

[25] E. Rico, T. Pichler, M. Dalmonte, P. Zoller, and S. Montangero, Phys. Rev. Lett. **112**, 201601 (2014).

[26] B. Buyens, J. Haegeman, K. Van Acoleyen, H. Verschelde, and F. Verstraete, Phys. Rev. Lett. **113**, 091601 (2014).

[27] S. Kühn, J. I. Cirac, and M.-C. Bañuls, Phys. Rev. A **90**, 042305 (2014).

[28] M. C. Bañuls, K. Cichy, J. I. Cirac, K. Jansen, and H. Saito, Phys. Rev. D **92**, 034519 (2015).

[29] T. Pichler, M. Dalmonte, E. Rico, P. Zoller, and S. Montangero, Phys. Rev. X **6**, 011023 (2016).

[30] B. Buyens, J. Haegeman, H. Verschelde, F. Verstraete, and K. Van Acoleyen, Phys. Rev. X **6**, 041040 (2016).

[31] M. C. Bañuls, K. Cichy, K. Jansen, and H. Saito, Phys. Rev. D **93**, 094512 (2016).

[32] B. Buyens, F. Verstraete, and K. Van Acoleyen, Phys. Rev. D **94**, 085018 (2016).

[33] M. C. Bañuls, K. Cichy, J. I. Cirac, K. Jansen, and S. Kühn, Phys. Rev. Lett. **118**, 071601 (2017).

[34] B. Buyens, S. Montangero, J. Haegeman, F. Verstraete, and K. Van Acoleyen, Phys. Rev. D **95**, 094509 (2017).

[35] K. Zapp and R. Orus, Phys. Rev. D **95**, 114508 (2017).

[36] E. Ercolessi, P. Facchi, G. Magnifico, S. Pascazio, and F. V. Pepe, arXiv:1705.11047.

[37] Z.-C. Gu and X.-G. Wen, Phys. Rev. B **80**, 155131 (2009).

[38] P. H. Ginsparg, in *Fields, Strings and Critical Phenomena (Les Houches 1988, Session XLIX)*, edited by E. Brézin and J. Zinn-Justin (Elsevier, Amsterdam, 1988).

[39] J. L. Cardy, J. Phys. A **19**, L1093 (1986).

[40] J. L. Cardy, J. Phys. A **20**, 5039 (1987).

[41] L. V. Avdeev, J. Phys. A **23**, L485 (1990).

[42] K. Nomura, Phys. Rev. B **48**, 16814 (1993).

[43] R. Kenna, C. Pinto, and J. C. Sexton, Phys. Lett. B **505**, 125 (2001).

[44] G. Evenbly and G. Vidal, Phys. Rev. Lett. **115**, 180405 (2015).

[45] S. Yang, Z.-C. Gu, and X.-G. Wen, Phys. Rev. Lett. **118**, 110504 (2017).

[46] L. Ying, Multiscale Model. Simul. **15**, 1423 (2017).

[47] M. Bal, M. Mariën, J. Haegeman, and F. Verstraete, Phys. Rev. Lett. **118**, 250602 (2017).

[48] M. Hauru, C. Delcamp, and S. Mizera, Phys. Rev. B **97**, 045111 (2018).